journal

J. Am. Ceram. Soc., 92 [7] 1574–1579 (2009)
DOI: 10.1111/j.1551-2916.2009.03049.x

Sintering Mechanisms of Zirconium and Hafnium Carbides Doped with $MoSi_2$

Laura Silvestroni,[†,‡,§,¶] Diletta Sciti,[‡] Jens Kling,[§] Stefan Lauterbach,[§] and Hans-Joachim Kleebe[§]

[‡]CNR-ISTEC, Institute of Science and Technology for Ceramics, Via Granarolo 64, I-48018 Faenza, Italy

[§]TUD-IAG, Institute of Applied Geosciences, Schnittspahnstraße 9, D-64287 Darmstadt, Germany

[¶]Department of Industrial Chemistry and Materials, University of Bologna, Via Risorgimento 4, I-40136 Bologna, Italy

The microstructure of two pressureless-sintered ultra-high-temperature ceramics, namely ZrC+20 vol% $MoSi_2$ and HfC+20 vol% $MoSi_2$, was characterized by scanning and transmission electron microscopy. With regard to the ZrC–$MoSi_2$ system, Zr_xSi_y compounds and SiC were detected. In the HfC–$MoSi_2$ system, a mixed phase was detected at the triple points and identified as $(Mo,Hf)_5Si_3$. For both the systems investigated, the high wettability of the silicide-based phases on the matrix grains suggests that sintering is assisted by a liquid phase. This contribution reports for the first time on the sintering mechanisms of early transition metal carbides doped with $MoSi_2$ as a sinter additive, on the basis of the microstructural evolution observed upon sintering and in the light of phase diagrams and thermodynamical calculations.

I. Introduction

Zirconium and hafnium carbide (ZrC and HfC) are candidate materials for ultra-high-temperature structural applications due to their high melting point of 4173° and 3693°C, respectively,[1] and their capability to withstand temperatures exceeding 1600°C in an aggressive environment. They possess interesting engineering properties, such as high hardness (ZrC: ~25.5 GPa; HfC: ~20.0 GPa),[2] high electrical conductivity, and a high elastic modulus (ZrC: 400–440 GPa; HfC: 425 GPa).[2,3] ZrC is suitable for electronic applications, as thermoionic emitters, and nuclear applications, as a diffusion barrier for fission metals in the coatings of nuclear fuels. HfC is presently considered as a potential candidate material for aerospace applications as well as for a variety of applications including cutting tools, high-temperature shielding, field emitter tips, and arrays.[4,5]

Despite possessing useful properties, the use of monolithic carbides is strongly limited because of their poor sinterability and high machining costs. Several attempts have been made in order to decrease the sintering temperature, the applied pressure, and the amount of secondary phase required to achieve full density. Recently, it has been demonstrated that amounts of $MoSi_2$ ranging from 5 to 20 vol% promote the sinterability of TiB_2,[6] ZrB_2,[7,8] HfB_2,[8] ZrC,[9] and HfC[10] at temperatures in the range 1800°–2000°C, even without the application of pressure. However, the densification mechanisms are still unclear and under debate.

Transmission electron microscopy (TEM) is a powerful tool to explore microstructures on a small length scale to disclose the effective densification mechanisms. A thorough literature analysis revealed that neither detailed TEM work nor reports on densification mechanisms are available for this class of materials, which, however, are essential to optimize the sintering aids utilized and the processing parameters applied.

In the present study, the microstructure development of ZrC–$MoSi_2$ and HfC–$MoSi_2$ composites was carefully analyzed in order to gain an insight into the densification mechanisms occurring during pressureless sintering.

II. Experimental Procedure

The compositions under investigation are indicated in Table I. Details on the powder processing and sintering conditions are reported elsewhere.[9,10] For the sake of clarity, the impurities present in the commercial powders are also reported in Table II. To identify the crystalline phases formed, all samples were examined using X-ray diffraction (Siemens D500, Karlsruhe, Germany), with Cu$K\alpha$ radiation, a stepsize of 0.04, and a 1 s counting rate. The microstructures were analyzed on polished and fractured surfaces by scanning electron microscopy (SEM, Cambridge S360, Cambridge, U.K.) and energy-dispersive X-ray spectroscopy (EDS, INCA Energy 300, Oxford instruments, Tubney Woods, Abingdon, Oxfordshire, U.K.). In order to limit lateral spreading of the electron beam, EDS analysis was carried out at acceleration voltages $\leq$6 keV. TEM samples were prepared by cutting 3 mm disks from the sintered pellets. These were mechanically ground down to about 20 μm and then further ion beam thinned until small perforations were observed by an optical microscope. The detailed phase analysis was performed using TEM operating at 120 kV (FEI CM12 STEM, Eindhoven, the Netherlands) equipped with an energy-dispersive detector system (EDAX Genesis 2000, Amtek GmbH, Wiesbaden, Germany). Quantitative calculations of the microstructural parameters, like residual porosity and secondary phase content, were carried out via image analysis with a commercial software package (Image Pro-plus 4.5.1. Media Cybernetics, Silver Springs, MD).

III. Results

In Fig. 1, the fractured surfaces of pure ZrC and HfC materials are presented for comparison. The monoliths of undoped ZrC and HfC were pressureless sintered under identical sintering conditions as composites prepared with the addition of $MoSi_2$; however, their density retained values of approximately 70% of the theoretical density.

(1) ZrC- 20 vol% $MoSi_2$

This material showed good sinterability and the final density was 6.22 g/cm^3. The crystalline phases detected after sintering were cubic ZrC, tetragonal $MoSi_2$, and traces of β-SiC

R. Cutler—contributing editor

Manuscript No. 25624. Received December 11, 2008; approved February 20, 2009.
This work was supported by The Air Force Research Laboratory through the research grant FA8655-09-M-4002, in particular the contract monitor, Dr. Joan Fuller.
[†]Author to whom correspondence should be addressed. e-mail: laura.silvestroni@istec.cnr.it

Table I. Composition, Sintering Parameters, Theoretical and Experimental Density, Weight Loss of the Two Carbide Composites

Sample	Composition (vol%)	Sintering (°C/min)	Theoretical density (g/cm^3)	Experimental density (g/cm^3)	Weight loss (%)
ZC20	ZrC+20 $MoSi_2$	1950/60	6.57	6.22	2.3
HC20	HfC+20 $MoSi_2$	1950/60	11.40	11.00	1.2

(Fig. 2(a)). For this composite, a weight loss of 2.3% was calculated, which was ascribed to the vaporization of volatile species (CO, SiO, and MoO_3)[11,12] and to the formation of SiC, which has a considerably lower density (3.2 g/cm^3) than the constituent phases.[13] An example of the fractured surfaces is shown in the SEM image of Fig. 3(a). The bright phase corresponds to ZrC grains, which have a mean grain size of 6 μm and a square shape; the gray phase with an irregular shape is $MoSi_2$. The dark agglomerates within the $MoSi_2$ phase are SiC particles; their amount was calculated to be about 1% by image analysis. The formation of SiC was attributed to the reaction between $MoSi_2$ and residual carbon present as an impurity in the starting ZrC powder (1.5 wt%). At the ZrC–$MoSi_2$–SiC interface (see Fig. 3(b)), zirconium silicides with different stoichiometries and oxygen impurities were detected by EDS, which showed very low dihedral angles, suggesting that these silicide-based phases were liquid at the sintering temperature.

Further details on the microstructure were evidenced by TEM analyses. The bright-field image of the composite in Fig. 4 shows a ZrC grain and a bright SiC platelet embedded in the Zr_2Si phase. The substructure visible in the ZrC grains consists of a network of dislocations. In $MoSi_2$ grains, the formation of nanoprecipitates was observed to give rise to a necklace of dislocations. In Fig. 5, a mixture of reaction products is shown. TEM–EDS analyses confirmed the presence of ZrSi and $ZrSi_2$ phases with sharp boundaries. The presence of $MoSi_2$ in this area suggests that this was the original phase in which the reaction products formed. It should be noted that, going from $MoSi_2$ toward ZrC, zirconium silicides with a decreasing amount of silicon in their stoichiometry formed, suggesting a diffusion process as the underlying formation mechanism.

EDS spectra recorded from ZrC grains were superimposed onto the theoretical ZrC spectrum and, as can be seen in Fig. 6(a), the fit is not perfect. However, when Mo is included in the simulation (Fig. 6(b)), the calculated profile matches the experimental spectrum well. According to quantitative analyses, the estimated amount of Mo is about 3–4 at.%. Recent studies confirmed that Mo has a solubility in ZrC from 1.1 to 9.4 mol%.[14] On the other hand, the presence of Zr peaks was

Table II. Characteristics of the Commercial Powders Utilized for the Production of the Composites

Powder	Crystal structure	Supplier	Mean grain size (μm)	Particle size range (μm)	Impurities (wt%)
ZrC	Cubic	H.C. Starck (Karlsruhe, Germany), Grade B	3.8	0.8–8.0	C_{free}: 1.5 O: 0.6 N: 0.8 Fe: 0.05 Hf: 2
HfC	Cubic	Cerac Inc. (Milwaukee, WI)	0.8	0.2–1.5	U: 0.0002 Zr: <0.6
$MoSi_2$	Tetragonal	Aldrich (Milwaukee, WI)	2.8	0.3–5.0	O:1

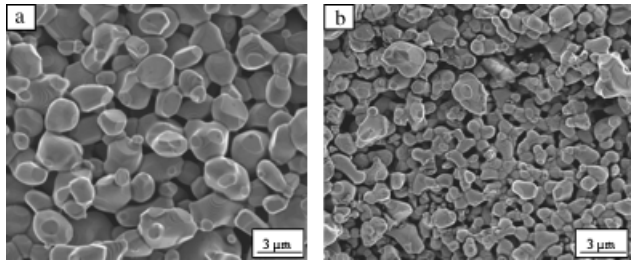

Fig. 1. Fractured surfaces of (a) ZrC and (b) HfC monoliths, which were pressureless sintered at 1950°C, 60 min.

detected in the $MoSi_2$ EDX spectra, indicating a mutual interdiffusion of Zr and Mo into the adjacent phases.

(2) HfC–$MoSi_2$

Similar to the ZrC-based composite, this material showed good sinterability. The final relative density was 11.00 g/cm^3 and SEM analysis confirmed that the residual porosity was 4%. During sintering, a weight loss of about 1.2% occurred and it was shown during previous experiments to be linear with increasing additive amount.[10]

The XRD pattern acquired from the HfC-based composite revealed the presence of cubic HfC and tetragonal $MoSi_2$ (Fig. 2(b)). Despite collecting the pattern at a slower accumulation time, no trace of other phases was detected within the detection limit of XRD.

A characteristic example of the microstructure is shown in Fig. 7(a): HfC grains appear bright with a faceted shape homogeneously distributed with the dark $MoSi_2$ phase. This microstructure reveals that where the amount of $MoSi_2$ is more abundant, the grains retained a round shape and a dimension around 1 μm, while where the sintering additive was scarce, the grains grew in dimensions up to 10 μm. This feature indicates that $MoSi_2$ could act as a grain growth inhibitor for HfC if the dispersion of the secondary phase is improved. Analogous to the ZrC system, mixed phases based on Hf–Mo–Si were detected by EDS analyses, among HfC grains (Fig. 7(b)). The formation of these phases suggests a mutual solubility between the two main phases and their shape, with very low dihedral angles, indicates crystallization from the liquid phase.

A detailed microstructural characterization by TEM did not reveal any dislocations in HfC grains, but strain contrasts were often noticed. TEM–EDX analyses confirmed the formation of

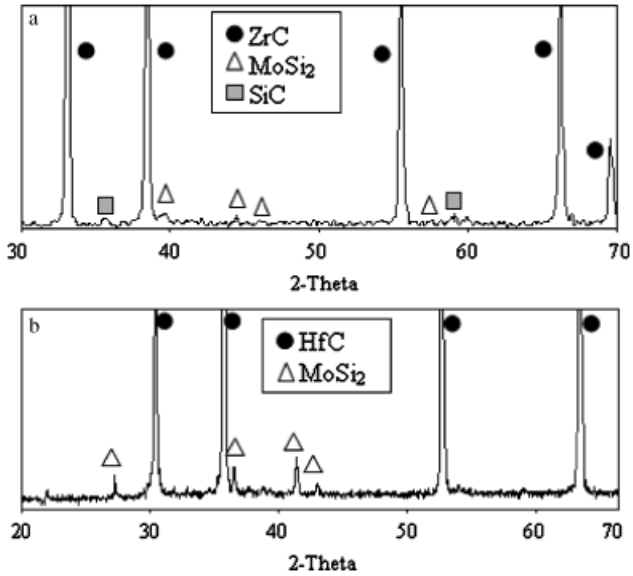

Fig. 2. X-ray diffraction pattern of (a) the ZrC-20 vol% $MoSi_2$ composite and (b) the HfC-20 vol% $MoSi_2$ composite.

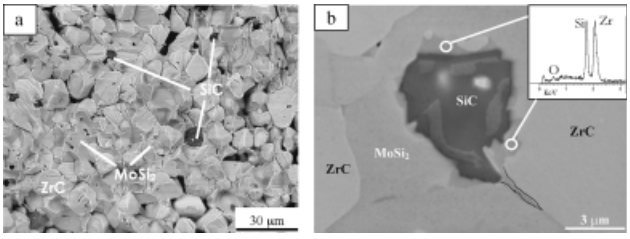

Fig. 3. Scanning electron microscope images of the ZC20 material: (a) fractured surface and (b) higher magnification of the polished surface; note the low dihedral angle of the Zr–Si phase.

a $(Hf,Mo)_xSi_y$ phase at the triple point junctions (see an example in Fig. 8). This aspect reveals a partial substitution of Hf into Mo sites. Oxygen impurities were also observed, as shown in the EDS spectrum in Fig. 8. The interfaces of this mixed $(Hf,Mo)_xSi_y$ phase are concave toward HfC and convex toward $MoSi_2$, suggesting a wetting tendency only toward the silicide. In fact, the HfC–HfC grain-boundaries were clean with plane interfaces. The size of the crystalline phase at a triple pocket varies between 150 and 200 nm. Two configurations of the triple point junctions were observed: in one case, at least one of the surrounding grains was $MoSi_2$, while in many other cases all the three adjacent grains were HfC. The composition of the mixed phase was calculated by EDS analyses on several triple points and different stoichiometries were detected. Most of the triple points had an average composition of Mo = 32, Hf = 32, and Si = 36 at.%. If we assume that the transition metal atoms substitute Mo within the unit cell, as reported by Sakida *et al.*,[15] then the ratio metal/metalloid would be approximately 64/36. In addition, if we consider the phases in the system Hf–Si with a close ratio, then the possible phases are Hf_2Si (66.7/33.3) and Hf_5Si_3 (62.5/37.5). In order to identify these mixed phase, several electron diffraction patterns were taken from one single grain with different tilting angles. The analysis of the *d*-values calculated from the diffraction patterns indicated that the $(Hf,Mo)_xSi_y$ phase had a structure not referable to the *d*-values of the known Mo–Si or Hf–Si phases. To experimentally obtain the cell constants, the parameters obtained from the diffraction patterns were checked with respect to tilting angles. The resulting unit cell has a hexagonal structure with $a = 740$ pm and $c = 520$ pm. Both the structure and the lattice constants are very close to the hexagonal Hf_5Si_3 with the space group n° $P6_3/mcm$ and lattice parameters of $a = 789.0$ pm and $c = 555.8$ pm.

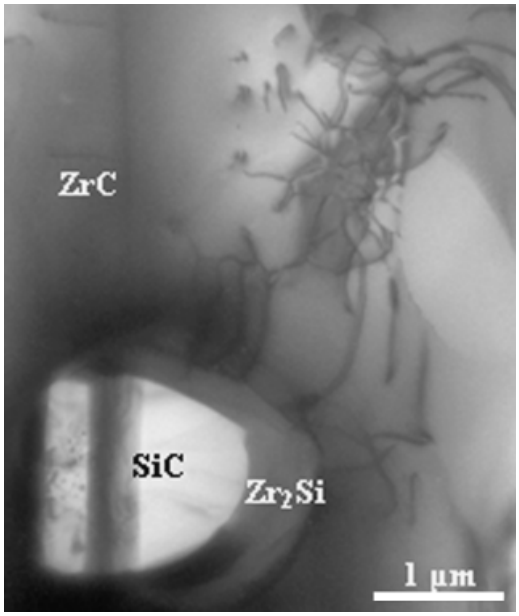

Fig. 4. BF-TEM image of a ZC20 composite showing the formation of SiC adjacent to the Zr_2Si phase.

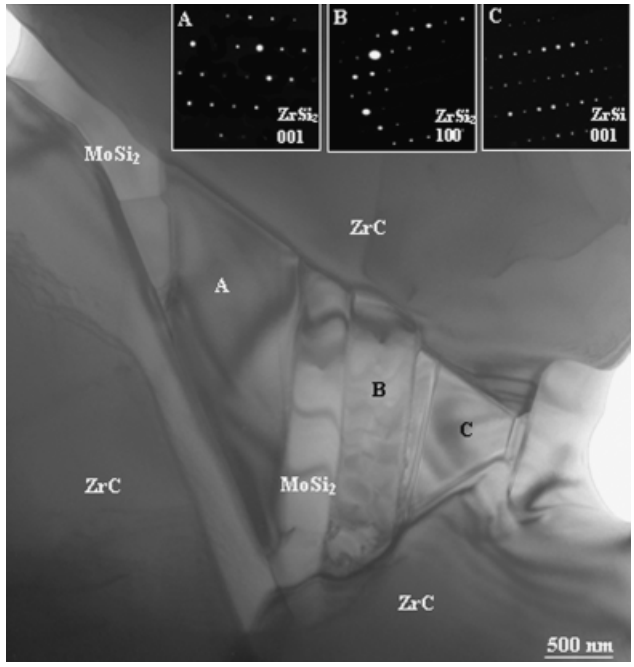

Fig. 5. BF-TEM image of a ZC20 material where $ZrSi_2$ and ZrSi phases coexist. A diffraction pattern for each phase is shown in the insets.

IV. Discussion

The most relevant data emerged from this investigation, which will be useful to understand the sintering mechanisms and the crucial roles of metal silicides in the densification of these covalent compounds are the following:

(1) In ZrC–$MoSi_2$ material, Zr_xSi_y products were found at the interface between the two main phases and they were identified as $ZrSi_2$, ZrSi, and Zr_2Si.

(2) Analogous to the ZrC–$MoSi_2$ system, small amounts of Hf–Mo–Si phase were detected besides HfC and molybdenum disilicide at triple point junctions in the HfC–$MoSi_2$ system.

From these observations, we can conclude that Zr and Hf have at least a limited solubility in Mo silicides and that Zr has a higher mobility than Hf, because pure zirconium silicides were detected compared with the mixed Hf–Mo–Si phase. Besides, the presence of only a very limited amount of secondary phases, detected at the triple point junctions, suggests that the active species could be Mo_5Si_3 instead of $MoSi_2$, a phase that is always present as an impurity.

One possible formation mechanism of these phases could be explained by the substitution of Zr or Hf at Mo sites into Mo_5Si_3, leading to the formation of Zr_5Si_3 or Hf_5Si_3. Some arguments in favor of or against this hypothesis are considered.

(1) A necessary but not sufficient condition is the phase stability criterion with respect to the size factor, which refers to the

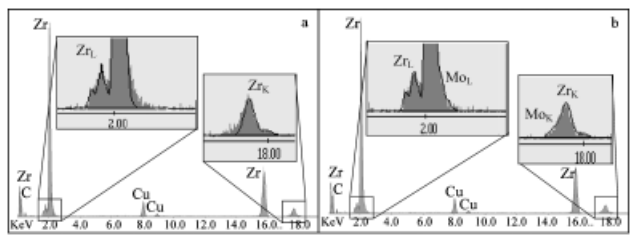

Fig. 6. Energy-dispersive X-ray spectra of ZrC grains and the calculated spectra superimposed including Zr–C in (a) and Zr–Mo–C in (b).

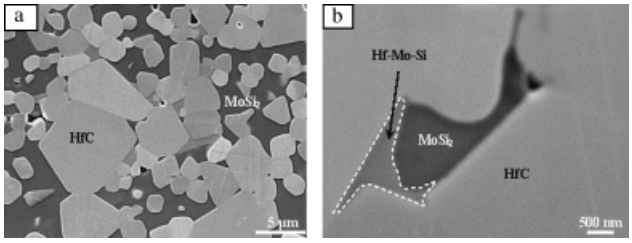

Fig. 7. Scanning electron microscopy image of HC20 material at (a) a lower and (b) a higher magnification, revealing the formation of an Hf–Mo–Si secondary phase.

15% Hume–Rothery rule.[16] If we consider the atomic radius of Mo equal to 130 pm,[17] then the range of atomic radius that can be accommodated in the silicide at Mo sites is compatible with the atomic radius of Zr and Hf with 145 and 144 pm, respectively.[17]

(2) Another favorable factor is the crystal structure. Like many other silicides, Mo_5Si_3 typically crystallizes in either a tetragonal or a hexagonal structure.[18] The body-centered tetragonal structure has the space group $I4/mcm$ and lattice parameters equal to $a = 964.8$ pm and $c = 491.4$ pm (PDF #34-0371). Minimum addition of carbon destabilizes the tetragonal structure and results in the formation of a carbon-stabilized hexagonal Nowotny phase.[19] The hexagonal phase is characterized by the space group $P6_3/mcm$ and lattice parameters equal to $a = 729$ pm and $c = 500$ pm.[20] Both Zr_5Si_3 and Hf_5Si_3 have a hexagonal structure with the space group $P6_3/mcm$ and lattice parameters $a = 788.5$ pm and $c = 555.8$ pm (PDF #06-0582) and $a = 789.0$ pm and $c = 555.8$ pm (PDF #12-0468), respectively. The shift from a tetragonal to a hexagonal structure would imply a distortion of the cell from 90°–90° to 60°–120°, but if we consider a transition from the Nowotny phase to Zr_5Si_3 or Hf_5Si_3, then the same hexagonal crystal structure is preserved. In both cases, the orientation of the crystal with an elongated a-axis is maintained.

(3) Calculations of the covalent and molecular volumes favor a Transition Metal/Mo substitution, because both $MoSi_2$ and tetragonal Mo_5Si_3 have a molecular volume lower than the covalent volume (−2% and −12%, respectively), which implies a cell with free space available for atoms with a larger steric hindrance, such as Zr and Hf. On the other hand, the hexagonal Mo_5Si_3 shows the opposite tendency; the covalent volume exceeds the molecular volume of about 5% and consequently it should not be prone to the substitution.

(4) The last consideration relates to the mixed Hf–Mo–Si phase observed in the HfC–$MoSi_2$ material. Because the parameters calculated for this phase are very close to the Hf_5Si_3 lattice, the substitution of Mo by Hf in Mo_5Si_3 is highly probable.

The hypotheses of cation transfer, diffusion, and a change in the crystal structure are strongly promoted by the presence of a liquid phase. Hence, it is worth pointing out the possible origin of liquid formation based on phase diagram considerations.

From the Mo–Si phase diagram in Fig. 9(a), redrawn from,[21] we can see that below the sintering temperature, if the actual composition slightly differs from the peritectic composition of either $MoSi_2$ or Mo_5Si_3, we have compresence of a liquid phase and, at a composition of 55 at.% of Si, eutectic liquid is predicted at 1910°C between $MoSi_2$ and Mo_5Si_3. Because the sintering temperature is 1950°C, we see that there is a high probability of formation of a liquid phase during sintering.

Another useful diagram is the one reported by Fan *et al.*[22] where $MoSi_2$ and C are considered (compare Fig. 9(b)). Above 1700°C, SiC formation and the presence of a liquid phase are predicted at any C/$MoSi_2$ ratio.

The melting points and onset temperatures of liquid-phase formation in the Zr–Si and Hf–Si systems are summarized in Table III.[23,24] The eutectic temperature of a number of compositions is below the sintering temperature (1950°C) and hence a liquid phase must be present during densification. Thus, microstructural features in combination with the phase diagrams strongly suggest that densification of ZrC–$MoSi_2$ and HfC–$MoSi_2$ composites is promoted by a liquid phase, involving rearrangement of grains and matter transfer via the transient liquid. Besides, oxygen impurities detected by EDS in all the silicides confirm their important role of oxygen removal from the matrix, which is well known to hinder the densification of UHTCs.[25] However, the reaction path leading to the formation of the observed phases remains to be determined.

For this purpose, the thermodynamics of these systems is considered. Because of lack of data on HfC–$MoSi_2$ interactions, only the ZrC–$MoSi_2$ system will be discussed in light of thermodynamical calculations performed with a commercial software.[26] The starting hypotheses are atmospheric pressure, a C-rich environment, and interdiffusion of the cations. The changes in Gibbs free energy values as a function of temperature for the reactions considered are plotted in Fig. 10. The free energy calculation for the reaction between ZrC and $MoSi_2$ (Reaction (1)), which leads to $ZrSi_2$, indicates a positive free energy at the sintering temperature of 1950°C; hence, it is not favorable.

$$ZrC + MoSi_2 = ZrSi_2 + MoC \quad (1)$$

Similarly, the diffusion of Zr into $MoSi_2$ (Reaction (2)), which leads to $ZrSi_2$ and Mo, is not thermodynamically allowed at and below 1950°C.

$$Zr + MoSi_2 = ZrSi_2 + Mo \quad (2)$$

However, because Zr_xSi_y species were observed in the final microstructure at the interface between ZrC and $MoSi_2$, other

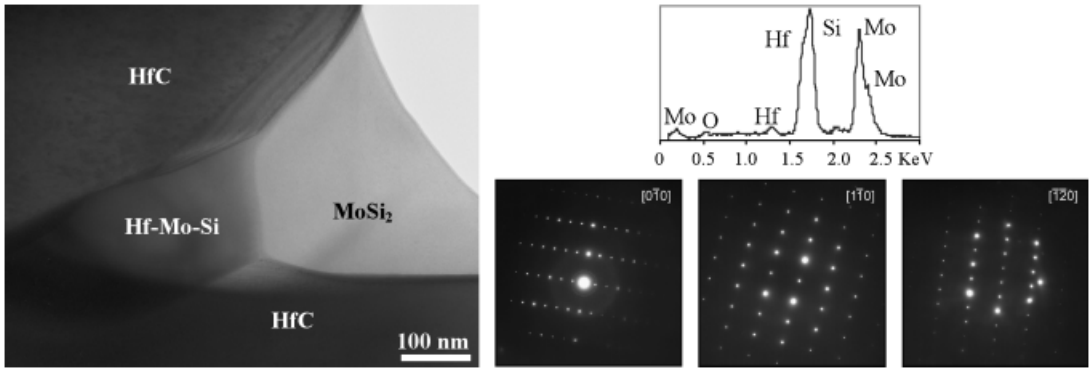

Fig. 8. Triple-point junction in HC20 material, the energy-dispersive X-ray spectrum of the mixed Hf–Mo–Si phase, and the corresponding diffraction patterns collected at different tilting angles.

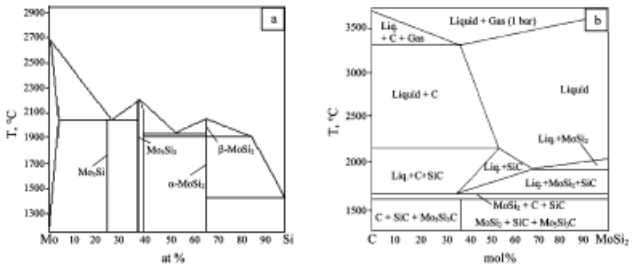

Fig. 9. (a) The Mo–Si phase diagram redrawn after Gokhale and Abbaschian[21] and (b) the $MoSi_2$–C pseudo-binary phase diagram redrawn after Fan *et al.*[22] This pseudo-binary phase diagram was observed by section through the C–Si–Mo ternary system along the C–$MoSi_2$ tie line at different temperatures, resulting in phase fields where three phases are in equilibrium.

reaction paths have to be figured out. Because of the highly reducing environment of the furnace[14] and the presence of pure carbon in the raw powders, the formation of Mo_5Si_3 and SiC is favorable through reaction (3):

$$5MoSi_2 + 7C = Mo_5Si_3 + 7SiC \quad (3)$$

As the Mo_5Si_3 phase was never observed in the microstructure of the ZrC-based composite, it is likely that Mo is replaced by Zr to yield Zr_5Si_3, as indicated by Reaction (4) ($\Delta G < 0$ at all temperatures):

$$5Zr + Mo_5Si_3 = Zr_5Si_3 + 5Mo \quad (4)$$

The Zr–Si phase diagram[23] indicates that Zr_5Si_3 is liquid at the sintering temperature. Hence, it can flow into the microstructure, filling voids among matrix grains favoring matter transport. When this phase comes in contact with a carbon source (Reaction (5)), the formation of Zr_2Si and SiC is predicted from a thermodynamical calculation:

$$2Zr_5Si_3 + C = 5\,Zr_2Si + SiC \quad (5)$$

The overall free energy for this reaction at 1950°C is estimated to be −313.7 kJ. If, instead, a source of silicon is close to

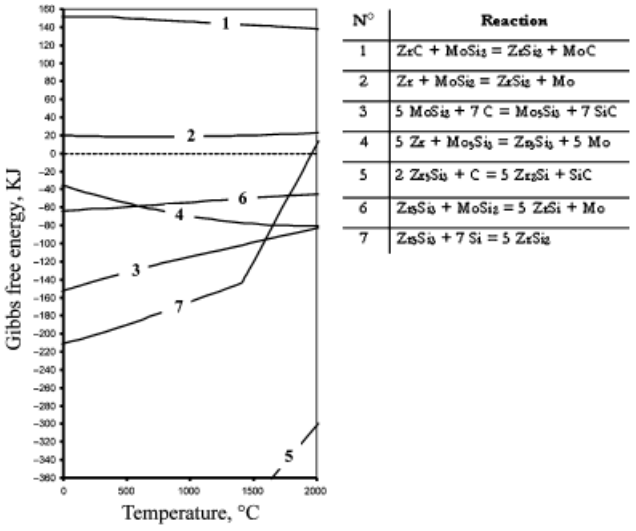

N°	Reaction
1	$ZrC + MoSi_2 = ZrSi_2 + MoC$
2	$Zr + MoSi_2 = ZrSi_2 + Mo$
3	$5\,MoSi_2 + 7\,C = Mo_5Si_3 + 7\,SiC$
4	$5\,Zr + Mo_5Si_3 = Zr_5Si_3 + 5\,Mo$
5	$2\,Zr_5Si_3 + C = 5\,Zr_2Si + SiC$
6	$Zr_5Si_3 + MoSi_2 = 5\,ZrSi + Mo$
7	$Zr_5Si_3 + 7\,Si = 5\,ZrSi_2$

Fig. 10. Plot of the possible reactions in the system ZrC–$MoSi_2$ calculated at ambient pressure: Gibbs free energy as a function of the temperature.

Table III. Melting or Decomposition Temperatures and Corresponding Eutectic or Peritectic Temperatures (Liquid Formation) in the Systems Zr–Si and Hf–Si[23,24]

System	Phase	Melting/decomposition T (°C)	Eutectic/peritectic T (°C)
Zr–Si	Zr_3Si	1650	1570
	Zr_2Si	1925	1650
	Zr_5Si_3	2180	1925
	Zr_3Si_2	2215	2215
	Zr_5Si_4	2250	2215
	ZrSi	2215	1620
	$ZrSi_2$	1620	1370
Hf–Si	Hf_2Si	2083	1828
	Hf_5Si_3	2357	2083
	Hf_3Si_2	2480	2320
	Hf_5Si_4	2313	2133
	HfSi	2133	1546
	$HfSi_2$	1546	1325

Zr_5Si_3, it will react to form ZrSi and $ZrSi_2$ according to Reactions (6) and (7), as follows:

$$Zr_5Si_3 + MoSi_2 = 5ZrSi + Mo \quad (6)$$

$$Zr_5Si_3 + 7Si = 5ZrSi_2 \quad (7)$$

Excess molybdenum, as derived from Reactions (4) and (6), can oxidize to volatile MoO_3 or can be incorporated into the ZrC lattice, forming solid solutions as confirmed by EDS analysis (see Fig. 6). As shown in Fig. 10, reactions (3)–(7) discussed above are feasible and the products, according to the Zr–Si binary phase diagram, are liquid at the sintering temperature applied (see Table III).

Concerning the HfC–$MoSi_2$ system, an analogous behavior is assumed, activated by the formation of Mo_5Si_3, followed by a partial substitution of Hf on Mo sites. Moreover, Hf–Si compounds are liquid below the sintering temperature.

It may be possible that Zr- or Hf-silicides could have formed due to a solid-state reaction during heating of the powder compact at a lower temperature. Considering the binary phase diagrams of a system based on Mo, Si, Hf, Zr, and C,[21–24] it is evident that the transition metal silicides, even if formed in the solid state, would melt (melting temperatures ranging between 1390° and 2000°C) and form a liquid at 1950°C. TEM investigations revealed that these phases were present at triple pockets in the sintered microstructure, due to the migration of the liquid phase to those pockets during sintering. The segregation of all the silicides in the solid state to the triple points is rather unlikely due to the sluggish solid-state diffusion.

All the aforementioned observations led to a new picture regarding the effective role of $MoSi_2$ upon densification of ultra-high-temperature ceramics, involving liquid formation, chemical reactions, and cation diffusion at sintering temperature.

V. Conclusions

Based on the present results, it is concluded that:

(1) Densification of Hf and Zr carbides doped with $MoSi_2$ does occur via liquid-phase sintering, which is constituted by transition metal silicides.

(2) Mo_5Si_3 is likely to be the starting phase for the formation of Zr–Si or Hf–Si species as it has a larger solubility for IV Group transition metal carbides than $MoSi_2$.

(3) Local Mo_5Si_3 formation may occur through different mechanisms: it is already present in the starting powder due to $MoSi_2$ oxidation or could form through a reaction with C impurities.

(4) Zr completely substitutes Mo in Mo_5Si_3 and forms Zr_5Si_3, which in turn is transformed into Zr_2Si (if next to C

sources) or ZrSi and $ZrSi_2$ (if next to Si sources). Therefore, neither Mo_5Si_3 nor Zr_5Si_3 were found in the final microstructure.

(5) Hf has a lower mobility than Zr and only partially substitutes Mo sites in the Mo_5Si_3 structure and hence $(Hf, Mo)_5Si_3$ was observed in the final microstructure.

Acknowledgments

One of the authors, L.S., wishes to express her gratitude to Mathis Müller for his valuable help in TEM specimens' preparations and Giancarlo Celotti for the useful discussion on crystallography.

References

[1]H. Wiedemeier and M. Singh, "Thermochemical Modelling of Interfacial Reactions in Molybdenum Disilicide Matrix Composites," *J. Mater. Sci.*, **27** [11] 2974–8 (1992).

[2]A. Krajewski, L. D'Alessio, and G. De Maria, "Physico–Chemical and Thermophysical Properties of Cubic Binary Carbides," *Cryst. Res. Technol.*, **33** [3] 341–74 (1998).

[3]H. O. Pierson, *Handbook of Refractory Carbides and Nitrides*. William Andrew Publishing/Noyes, Westwood, NJ, U.S.A., 1996, 68pp.

[4]A. Sayir, "Carbon Fiber Reinforced Hafnium Carbide Composite," *J. Mater. Sci. Lett.*, **39** [19] 5995–6003 (2004).

[5]M. M. Opeka, I. G. Talmy, E. J. Wuchina, J. A. Zaykoski, and S. J. Causey, "Mechanical, Thermal and Oxidation Properties of Refractory Hafnium and Zirconium Compounds," *J. Eur. Ceram. Soc.*, **19** [13–14] 2405–14 (1999).

[6]T. S. R. C. Murthy, B. Basu, and R. Balasubramaniam, "Processing and Properties of TiB_2 with $MoSi_2$ Sinter-Additive: A First Report," *J. Am. Ceram. Soc.*, **89** [1] 131–8 (2006).

[7]D. Sciti, S. Guicciardi, A. Bellosi, and G. Pezzotti, "Properties of a Pressureless Sintered ZrB_2–$MoSi_2$ Ceramic Composite," *J. Am. Ceram. Soc.*, **89** [7] 2320–2 (2006).

[8]L. Silvestroni and D. Sciti, "Effects of $MoSi_2$ Additions on the Properties of Hf- and Zr–B_2 Composites Produced by Pressureless Sintering," *Scripta Mater.*, **57** [2] 165–8 (2007).

[9]L. Silvestroni and D. Sciti, "Microstructure and Properties of Pressureless Sintered ZrC-Based Materials," *J. Mater. Res.*, **23** [7] 1882–9 (2008).

[10]D. Sciti, L. Silvestroni, and A. Bellosi, "High-Density Pressureless-Sintered HfC-Based Composites," *J. Am. Ceram. Soc.*, **89** [8] 2668–70 (2006).

[11]F. F. Lange, "Volatilization Associated with the Sintering of Polyphase Si_3N_4 Materials," *J. Am. Ceram. Soc.*, **65** [8] c120–1 (1982).

[12]R. F. Voitovich and E. A. Pugach, "High Temperature Oxidation Characteristics of the Carbides of the Group VI Transition Metals," *Powder Metall. Met. Ceram.*, **12** [4] 314–8 (1973).

[13]C. H. McMurtry, W. D. G. Boecker, S. G. Seshadri, J. S. Zanghi, and J. E. Garnier, "Microstructure and Material Properties of SiC-TiB_2 Particulate Composites," *Am. Ceram. Soc. Bull.*, **66** [2] 325–9 (1987).

[14]S. E. Landwhr, G. E. Hilmas, and W. G. Fahrenholtz, "Processing of ZrC–Mo Cermets for High Temperature Applications, Part I: Chemical Interactions in the ZrC–Mo System," *J. Am. Ceram. Soc.*, **90** [7] 1998–2002 (2007).

[15]R. Sakida and J. H. Perepezko, "Phase Stability and Alloying Behaviour in the Mo–Si–B System," *Metall. and Mater. Trans. A.*, **36** [3] 507–14 (2005).

[16]W. Hume-Rothery, *Atomic Theory for Students of Metallurgy* Monograph and Report Series No. 3, The Institute of Metals, London, 1969.

[17]P. Silvestroni, *Fondamenti di Chimica, (Chemical Foundamentals)*, p. 532. Veschi Editore, Roma, 1980.

[18]J. W. Martin (ed.) *Concise Encyclopedia of the Structure of Materials*. Elsevier, Amsterdam, 2006, 237pp.

[19]S. Jayashankar and M. J. Kaufman, "Tailored $MoSi_2$/SiC Composites by Mechanical Alloying," *J. Mater. Res.*, **8** [6] 1428–41 (1993).

[20]C. L. Fu, X. Wang, Y. Y. Ye, and K. M. Ho, "Phase Stability, Bonding Mechanism, and Elastic Constants of Mo_5Si_3 by First-Principles Calculation," *Intermetallics*, **7** [2] 179–84 (1999).

[21]A. B. Gokhale and G. J. Abbaschian, "The Mo–Si System," *J. Phase Equilib.*, **12** [4] 493–8 (1991).

[22]X. Fan, K. Kack, and T. Ishigawi, "Calculated C–$MoSi_2$ and B–Mo_5Si_3 Pseudo-Binary Diagrams for the Use in Advanced Materials Processing," *Mater. Sci. Eng. A*, **278** [1] 46–53 (2000).

[23]H. Okamoto, "The Zr–Si System," *Bull. Alloy Phase Diagrams*, **11** [5] 513–9 (1990).

[24]J.-C. Zhao, B. P. Bewlay, M. R. Jackson, and Q. Chen, "Hf–Si Binary Phase Diagram Determination and Thermodynamic Modeling," *J. Phase Equilib.*, **21** [1] 40–5 (2000).

[25]W. A. Zdaniewski and N. L. Brungard, "X-Ray Photoelectron-Spectroscopy Studies of Metallic Diborides," *J. Am. Ceram. Soc.*, **75** [10] 2849–56 (1992).

[26]F*A*C*T, Facility for the Analysis of Chemical Thermodynamics. Available at http://www.crct.polymtl.ca/fact/ (Fact-Web, 1996). □